

ON THE DYNAMICAL EVOLUTION OF THE ARCHES CLUSTER

SOURAV CHATTERJEE¹, SANGHAMITRA GOSWAMI¹, STEFAN UMBREIT¹, EVERT GLEBBEEK², FREDERIC A. RASIO¹, AND JARROD HURLEY³

¹ Department of Physics and Astronomy, Northwestern University, Evanston, IL 60208, USA

² Department of Physics and Astronomy, McMaster University, 1280 Main Street West, Hamilton, Ontario L8S 4M1, Canada and

³ Center for Astrophysics and Supercomputing, Swinburne University of Technology, VIC 3122, Australia

Draft version December 2, 2018

ABSTRACT

We study the dynamical evolution of the young star cluster Arches and its dependence on the assumed initial stellar mass function (IMF). We perform many direct N -body simulations with various initial conditions and two different choices of IMFs. One is a standard Kroupa IMF without any mass segregation. The other is a radially dependent IMF, as presently observed in the Arches. We find that it is unlikely for the Arches to have attained the observed degree of mass segregation at its current age starting from a standard non-segregated Kroupa IMF. We also study the possibility of a collisional runaway developing in the first $\sim 2-3$ Myr of dynamical evolution. We find that the evolution of this cluster is dramatically different depending on the choice of IMF: if a primordially mass segregated IMF is chosen, a collisional runaway should always occur between $2-3$ Myr for a broad range of initial concentrations. In contrast, for a standard Kroupa IMF no collisional runaway is predicted. We argue that if Arches was created with a mass segregated IMF similar to what is observed today then at the current cluster age a very unusual, high-mass star should be created. However, whether a collisional runaway leads to the formation of an intermediate-mass black hole (IMBH) depends strongly on the mass loss rate via winds from massive stars. Growth of stellar mass through collisions can be quenched by strong wind mass loss. In that case, the inter-cluster as well as intra-cluster medium are expected to have a significant Helium enrichment which may be observed via Helium recombination lines. The excess amount of gas lost in winds may also be observed via X-ray observations as diffused X-ray sources.

Subject headings: methods: N-body simulations, methods: numerical, globular clusters: individual (Arches), stellar dynamics

1. INTRODUCTION

One of the biggest uncertainties in star cluster evolution studies lies in determining the true initial stellar mass function (IMF). Traditionally all studies focusing on the dynamical evolution of star clusters assume an initially fully formed cluster with a given number of single and binary stars, all at zero age main sequence (ZAMS) at $t = 0$ and no gas. It is also often assumed that the IMF is a standard power-law (or power-laws with different indices in different mass ranges) with no primordial radial variation in the cluster (e.g., Salpeter 1959; Miller & Scalo 1979; Kroupa 2001). However, star formation simulations indicate that neither of the above simplifications may be valid. For example, star formation takes place over a time-period and the formation timescale depends on many different physical processes including the Jeans mass of the protostellar clouds, radiative feedback and turbulence (e.g., Tan et al. 2006). Moreover, depending on these detailed physical processes stars of different mass ranges may form over different timescales (e.g., Dib et al. 2007a; Krumholz et al. 2009). In addition, deviations from the standard MFs are observed in many clusters both at the high mass and the low mass ends (e.g., Elmegreen 2004). In particular at the high mass end observed MFs are generally top-heavy compared to standard power-laws in dense cluster cores like the Arches cluster and starburst regions (Stolte et al. 2002; Kim et al. 2006; Dabringhausen et al. 2009). Mass segregation is also ob-

served in old globular clusters (e.g., Subramaniam et al. 1993; Hillenbrand & Hartmann 1998; Baumgardt et al. 2008). Whether the observed mass segregation is imprinted from the star formation epoch or it is attained via dynamical evolution of the cluster at a later time is still an open question. Although a conclusive general answer to this question does not exist, it has been shown in the case of the very young Trapezium cluster in the Orion nebula that the observed degree of mass segregation cannot be explained simply via dynamical mass segregation and a preferential formation of high-mass stars near the center is necessary to explain the observations (Bonnell & Davies 1998).

In order to bypass the above mentioned assumptions a detailed model for the star formation processes during the formation of the cluster is needed. Interstellar clouds contract and fragment due to density perturbations to form pre-stellar cores (PSC) that collapse on timescales that depend on their Jeans masses to form stars (e.g., Nakano 1966). Depending on the compactness of the assortment of these PSCs they can merge with other PSCs and grow before they collapse to form stars (e.g., Silk & Takahashi 1979; Elmegreen & Shadmehri 2003; Dib et al. 2007b). Using this simple model Dib et al. (2007a) have attempted to eliminate the above-mentioned assumptions regarding cluster IMFs by building an IMF from a distribution of PSCs in a molecular cloud. In their simplified model they assume that each PSC collapses to form a single star

of mass proportional to the parent PSC. Comparing the collision timescale between the PSCs with the collapse timescale of the PSCs they show that near the central regions of a dense cluster the PSCs collide and grow in mass before they can collapse to form a star. Thus, near the core where the number density of the PSCs is significantly higher than that in the halo, it is more likely to form stars that are heavier than stars formed from PSCs in the halo. Using the Arches cluster as a particular example they show that their semi-analytical model naturally results in a mass segregated cluster similar to the Arches cluster and the observed top-heaviness near the center is thus explained as imprinted from the star formation epoch.

The effects of primordial mass segregation on the global dynamical evolution of clusters have been explored previously in a parametric way showing interesting differences in the global properties of those clusters and their dynamical evolution (e.g., Baumgardt et al. 2008; Gürkan et al. 2004). The observed top-heavy MF in the central regions of the Arches cluster (e.g., Kim et al. 2006, 2007) thus makes it an interesting candidate for such studies. If the observed radially dependent top-heaviness in Arches MF is indeed primordial, then this is a direct measurement of the degree of mass segregation at formation of this cluster, thus it eliminates the necessity for parameterization.

The Arches cluster is also unique for the following reasons. The cluster has a projected distance of ~ 30 pc from the Galactic center (Nagata et al. 1995; Portegies Zwart et al. 2002; Kim et al. 2006, 2007). Estimates from detailed proper motion observations with a baseline of ~ 4 yr indicate that the real Galactocentric distance of the Arches cluster is ≈ 27 pc (Stolte et al. 2008). Thus the Arches is the closest massive cluster from the Galactic center. The proximity of the cluster from the Galactic center necessitates this cluster to be compact to be saved in the face of possible early tidal disruption. Serabyn et al. (1998) a decade ago found $\gtrsim 100$ O stars within 0.6 pc of the cluster, indicating Arches to be the densest young cluster in the Galaxy. The high estimated total cluster mass ($\sim 10^4 - 10^5 M_\odot$), and the high luminosity $10^8 L_\odot$ thus make this young cluster a power house cluster for Galactic standards (e.g., Serabyn et al. 1998). The central stellar density of the Arches cluster is $\sim 10^5 M_\odot/\text{pc}^3$ (e.g., Serabyn et al. 1998; Portegies Zwart et al. 2007), which is typical only for some old Galactic globular clusters. The core radius (r_c) of the Arches cluster is $\lesssim 0.2$ pc (e.g., Figer et al. 1999; Stolte et al. 2002; Stolte 2006). The high central density and the high mass thus makes the Arches cluster a very good candidate to study for possibility of collisional runaway. The Arches cluster is also very young, the cluster age (t_{cl}) is only 2 ± 1 Myr (e.g., Stolte et al. 2008). The timescale for a successful collisional runaway is only ~ 3 Myr since past that age, the cluster is depleted of its high-mass stars due to Supernova explosions (e.g., Freitag et al. 2006a, 2007). Hence, if conducive for a collisional runaway, the Arches cluster may be undergoing that process at the present time.

Two main scenarios to create the observed top-heavy radially dependent MF have been suggested in previous studies: 1. The observed MF is primordial, as men-

tioned earlier (e.g., Dib et al. 2007a). 2. The observed MF is a result of dynamical evolution starting from a standard IMF with no primordial radial variation (e.g., Portegies Zwart et al. 2007). Using numerous numerical simulations we study the dynamical evolution of the Arches cluster assuming the observed MF was indeed primordial. We compare the results from these simulations with the results from another set of simulations where the initial cluster properties are kept unchanged but a standard IMF with no radial variation is used instead. We investigate whether it is possible to attain the observed degree of mass segregation starting from an unsegregated cluster. We verify that the MFs and cluster parameters of the simulated clusters at $t_{cl} \approx 2$ Myr are consistent with observations. We then investigate the differences in the dynamical evolution of the simulated Arches-like clusters with the two above-mentioned choices of IMFs focusing on the possibilities of a collisional runaway. Furthermore, we study the final fate and discuss the possible observational signatures of a collisional runaway depending on the stellar wind prescription. The arrangement of this paper is as follows. In §2 we describe our simulations. In §3 we summarize our key results. This is followed by §4 where we discuss the key observable signatures of a collisional runaway. We summarize and conclude in §5.

2. INITIAL CONDITIONS

We simulate clusters consisting initially of 65536 stars with positions and velocities chosen according to a King profile (King 1966) with dimensionless central potential W_0 in the range from 5 to 9. The initial virial radius (r_v) of the cluster is set to 0.5 pc, which results in simulated clusters that have characteristic radii, e.g., r_c and tidal radius (r_t) at ≈ 2 Myr close to the observed values for the Arches cluster (Table 1, see also §1 for observed values). Our simulated clusters are initially Roche lobe filling. Numerical simulations by Gieles & Baumgardt (2008) show that dynamical evolution and tidal truncation makes initially underfilled and overfilled clusters Roche lobe filling and Roche lobe limited at timescales of the order of their half-mass relaxation time ($t_{r,h}$). Since the typical initial $t_{r,h}$ for our simulated Arches-like clusters is much lower ($\sim 10^3$ yr) than the current age of Arches, the above assumption is justified.

All the simulated clusters are assumed to be in a circular orbit around the Galactic center. Although the cluster orbit may be eccentric, the variations of its distance to the Galactic center are not expected to be significant for this study (Stolte et al. 2008). We simulate all clusters at a fixed Galacto-centric distance since given the present day mass and Galactic location of the Arches cluster, inspiral timescale from a larger distance is more than an order of magnitude longer than its estimated age (Gürkan & Rasio 2005; Stolte et al. 2008). One may argue however, that Arches initially was a lot more massive (needs to be $> 10^6 M_\odot$, Kim & Morris 2003) and has lost most of its mass during its evolution and inspiral and is now observed at its current position just before complete disruption. We find in our simulations that the total mass loss from escaping stars through the tidal boundary and from stellar evolution typically is only ~ 0.04 of the initial cluster mass during the first 2 Myr. Since, at the current position of Arches the tidal effects of the Galaxy is the maximum if inspiral scenario

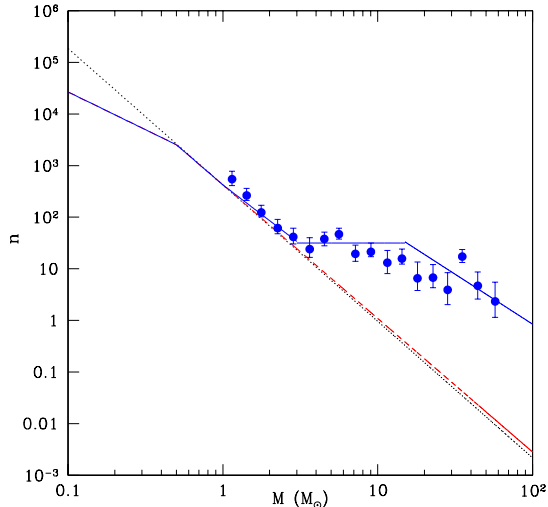


FIG. 1.— Comparison of the **Seg** IMF within $2r_c$ from the cluster center of mass with other standard IMFs and the observed data points. Black dotted line is the standard Salpeter IMF, red dashed line is the Kroupa (2001) IMF, and The Blue dots and the error-bars are extracted using ADS’s Dexter applet (Demleitner et al. 2001) from Dib et al. (2007a) showing the observed MF within $2r_c$ in Arches. The blue solid line is an approximation of the observed MF within $2r_c$ in the Arches cluster using broken power-laws of the form $n \propto M^{-\alpha}$, where α changes in different mass ranges. The α values are given in the form $M_1(\alpha)M_2$ in the mass range M_1 to M_2 in M_\odot : 0.1(1.3)0.5(2.3)1.0(2.04)3.0(0.15)(1.72)100. For $r > 2r_c$, the IMF **Seg** is standard Kroupa 2001.

is to be believed, this mass loss rate is an upper limit. Thus it is unlikely that Arches was initially more massive than $10^6 M_\odot$.

For each cluster profile we perform two sets of simulations using different IMFs to assign masses to stars. For the set of simulations with initially non-segregated clusters we use the IMF in Kroupa (2001) for the whole cluster (henceforth, **Nseg**). For the second set we choose a radially dependent IMF (henceforth, **Seg**), with a central top-heavy mass function for $r \leq 2r_c$, very similar to the observed one of Kim et al. (2006, Figure 1) and a standard Kroupa (2001) IMF outside. Initial cluster properties and key results are summarized in Table 1. In order to make sure that our results are robust against statistical fluctuations we repeat each simulation 2 times varying the random seed for generating the positions and velocities for each cluster with the same IMF and initial W_0 . In order to advance the clusters in time we use the direct N -body code NBODY4 (Aarseth 2003) which includes the tidal effects of the Galaxy, the evolution of stars using the integrated SSE/BSE package (Hurley et al. 2000, 2002), and makes use of the GRAPE6 hardware to speed-up the computation of the gravitational forces between stars. The evolution of each cluster is followed for 5 Myr, which is longer than the approximate time when the first supernova explosions occur, turning the most massive stars into black holes and consequently ending any possible runaway-growth (Freitag & Benz 2002; Freitag et al. 2006b,a). We do not have primordial binaries in our simulated clusters, although binaries created via three-body interactions are automatically included. The initial ~ 10 Myr evolution of a star cluster is dominated

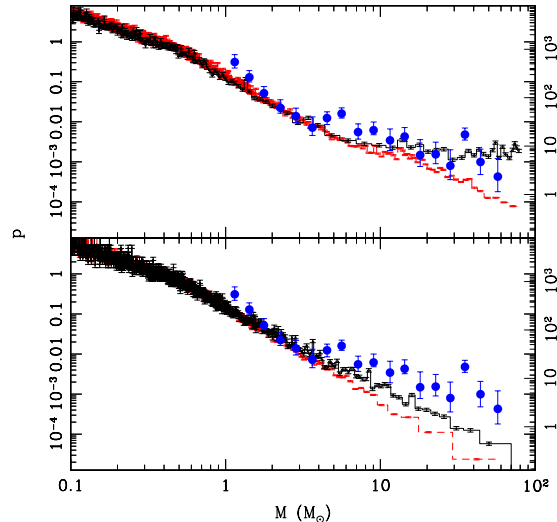


FIG. 2.— MFs of the simulated clusters for runs SW8-1 (top panel) and NSW8-1 (bottom panel) at 2.0 Myr. The red (dashed) and black (solid) histograms show MFs outside and inside $r = 2r_c$, respectively. The blue dots show the present day observed MF, taken from Dib et al. (2007a) using the Dexter application from ADS. The simulated histograms are normalized so that the area enclosed is unity. The observed points have the same normalization as used by Dib et al. (2007a, see right labels on the vertical axis). Both simulations show some degree of mass segregation. The primordially unsegregated cluster NSW8-1 do not attain the observed degree of mass-segregation at $t_{cl} = 2$ Myr. In contrast, the simulated MF matches the observed MF reasonably well for run SW8-1 with the primordially mass-segregated cluster with the **Seg** IMF.

by stellar evolution mass loss and two-body relaxation. Strong interaction mediated by binaries become a more important factor only at later times so far as the global evolution of the cluster is concerned. Including binaries, however, may decrease the mass segregation timescale and increase collision rate to some degree. Nevertheless, since the binary fraction in Arches is not known observationally, we choose not to consider primordial binaries rather than making a wild guess; the additional benefit is a significant reduction in computational cost.

3. RESULTS

In this section we present the results from our numerical simulations. We show in detail the results for clusters with $W_0 = 8$ and we summarize more briefly the results for all other runs.

3.1. Evolution of the Mass Function and Observational Constraints

Here we show, how well the initially segregated (**Seg**) and unsegregated (**Nseg**) cluster models can reproduce the observed level of mass segregation at the current age (2 Myr) of the Arches cluster. As a condition for consistency, the simulated clusters should have a present day MF consistent with the observed MF at the age of the Arches cluster. We compare the MF from the simulated clusters with (**Seg**) and without (**Nseg**) mass segregation at $t_{cl} = 2$ Myr with the observed MF. Figure 2 shows the MF within $r = 2r_c$ for runs SW8-1 and NSW8-1 at $t_{cl} = 2$ Myr. Each mass bin contains 50 stars so that the Poisson error is equal in each bin, and the MF is

TABLE 1
 LIST OF SIMULATIONS

Name	M ($10^4 M_\odot$) ^a		King W_0 ^b	IMF ^c	r (pc) ^d				M_{\max} (M_\odot) ^e	#Coll
	0 Myr	2 Myr			r_c	r_t	r_v	r_{hl}		
SW9-1	6.2	5.9	9		0.17 ± 0.05^f	19.7 ± 0.7	0.73 ± 0.03	1.14 ± 0.06	327, 252	19
SW9-2	6.3	6.1	9		0.12 ± 0.04	17.3 ± 0.6	0.66 ± 0.01	1.17 ± 0.07	356, - ^g	9
SW8-1	9.2	8.8	8		0.11 ± 0.03	15.2 ± 0.7	0.62 ± 0.01	0.74 ± 0.04	806, 326	30
SW8-2	9.0	8.6	8		0.07 ± 0.02	9.4 ± 0.5	0.48 ± 0.01	0.36 ± 0.02	1097, 647	47
SW7-1	9.2	8.9	7	Seg	0.10 ± 0.02	9.6 ± 0.3	0.49 ± 0.01	0.46 ± 0.02	683, 278	22
SW7-2	10.0	9.7	7		0.13 ± 0.04	10.8 ± 0.3	0.52 ± 0.01	0.55 ± 0.02	703, 428	15
SW6-1	12.8	12.4	6		0.10 ± 0.02	8.4 ± 0.2	0.46 ± 0.01	0.40 ± 0.02	140, 117	13
SW6-2	12.9	12.5	6		0.17 ± 0.01	8.7 ± 0.2	0.47 ± 0.01	0.44 ± 0.01	382, 144	26
SW5-1	15.9	15.3	5		0.19 ± 0.01	7.6 ± 0.2	0.43 ± 0.01	0.40 ± 0.01	126, 125	14
SW5-2	15.5	15.0	5		0.20 ± 0.01	7.4 ± 0.2	0.43 ± 0.01	0.39 ± 0.01	156, 107	13
NSW9-1	3.23	3.18	9		0.04 ± 0.01	12.0 ± 0.3	0.55 ± 0.01	0.8 ± 0.2	339, -	14
NSW9-2	3.20	3.18	9		0.04 ± 0.04	11.9 ± 0.2	0.55 ± 0.01	0.2 ± 0.2	238, 104	15
NSW8-1	4.2	4.1	8		0.18 ± 0.09	12.2 ± 0.8	0.55 ± 0.02	0.57 ± 0.06	136, 131	14
NSW8-2	3.2	3.2	8		0.06 ± 0.02	8.9 ± 0.2	0.47 ± 0.01	0.28 ± 0.06	135, -	8
NSW7-1	3.15	3.14	7	NSeg	0.08 ± 0.04	7.6 ± 0.1	0.4 ± 0.1	0.4 ± 0.1	-, -	8
NSW7-2	3.23	3.21	7		0.11 ± 0.03	7.6 ± 0.3	0.436 ± 0.008	0.24 ± 0.05	130, -	5
NSW6-1	3.3	3.2	6		0.08 ± 0.02	7.3 ± 0.1	0.426 ± 0.004	0.26 ± 0.02	116, -	2
NSW6-2	3.2	3.2	6		0.11 ± 0.02	6.8 ± 0.1	0.412 ± 0.003	0.37 ± 0.04	-, -	3
NSW5-1	3.2	3.1	5		0.15 ± 0.05	15.3 ± 0.5	0.62 ± 0.01	0.93 ± 0.07	233, 112	16
NSW5-2	3.2	3.2	5		0.08 ± 0.03	6.9 ± 0.1	0.42 ± 0.01	0.12 ± 0.02	147, 104	7

^a Bound mass at the age (t_{cl}) of the simulated cluster.

^b King profile (King 1966)

^c The range in mass is $[0.1 - 100] M_\odot$

^d at $t_{cl} = 2$ Myr

^e Highest mass reached for the two most massive stars in the simulation.

^f All quoted errors are 1σ error-bars from statistical fluctuations between the snapshots over which the cluster properties are averaged for the simulated clusters.

^g Mass does not grow above $100 M_\odot$ within 4 Myr

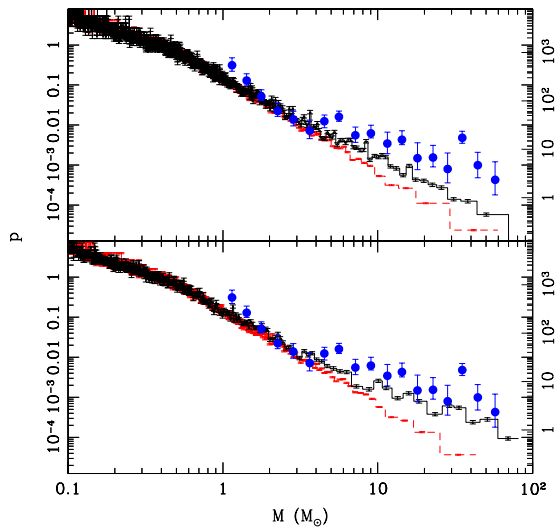


FIG. 3.— MFs of the simulated clusters for runs NSW8-1 with (top panel) and without (bottom panel) stellar evolution at 2.0 Myr. The red (dashed) and the black (solid) histograms show MFs outside and inside $r = 2r_c$, respectively. The blue dots show the present day observed MF, taken from (Dib et al. 2007a) using the Dexter application from ADS. The simulated histograms are normalized so that the area enclosed is unity. The observed points have the same normalization as used by Dib et al. (2007a, right labels on the y axis). In both cases the initial clusters are identical. The simulation including stellar evolution shows significantly lower degree of mass segregation than that without stellar evolution.

normalized such that its integral is unity. As it can be seen, while the evolved MF in the inner region of the Seg cluster is in good agreement with observations, this is not the case for the NSeg cluster. For the NSeg cluster the slope at the high mass end increases only marginally (from -2.3 to -1.6). While for the Seg cluster the MF becomes flatter, but remains still compatible with observations. Same results are obtained when the MFs are compared at $t_{cl} \approx 3$ Myr. This indicates that the degree of mass segregation observed in the Arches cluster is not likely to result simply from the cluster's dynamical evolution during its lifetime without any primordial mass segregation. It also indicates that, the MF at $t_{cl} = 2$ Myr for the simulated cluster is consistent if the observed MF of the Arches cluster truly is imprinted from its star formation epoch as suggested by Dib (2007).

We should note that for the NSeg IMF, a much higher degree of mass segregation can be achieved if stellar evolution is not included in the simulations. We find that if we turn off stellar evolution, the degree of flattening in the MF of the simulated cluster at ~ 2 Myr increases significantly compared to that with stellar evolution (Figure 3). Although the wind mass loss from the high-mass stars due to stellar evolution is negligible ($< 4\%$) compared to the total cluster mass in these simulations during the first 2 Myr, this mass is lost from the most massive stars in the cluster, which in turn reside near the center due to mass segregation. Thus this mass is lost from the deepest part of the cluster potential and can have a perceptible effect on the global properties of the cluster. From our results we conclude that the mass loss via stellar evolution from the massive stars can inhibit mass segregation

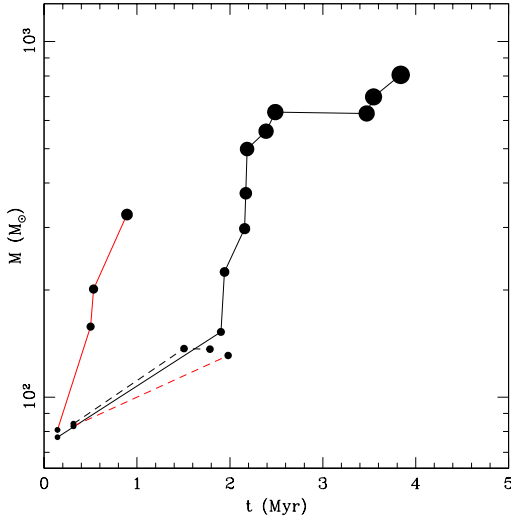


FIG. 4.— The growth of mass in time for the two most massive stars in the cluster are plotted for runs SW8-1 (solid lines) and NSW8-1 (dashed lines). Each dot denotes the time when the particular star changed mass through collision. The area of each dot is proportional to the stellar mass. For the **Seg** IMF a collisional runaway is observed starting around 2 Myr. For the **NSeg** IMF using the same initial conditions there is no runaway.

to a certain extent and simulations done without taking that physical effect into account will overestimate the amount of mass segregation. Since this effect is only predominant for the most massive stars at a given time in the cluster, the quantitative effect will depend on the number of high-mass stars present in the cluster. Despite a lower total number of initial stars ($N \approx 12K$ and $24K$), simulations in Portegies Zwart et al. (2007) had more massive stars than our **NSeg** clusters because of the truncated IMF they used. Thus, if stellar evolution is included, mass segregation should have been even more strongly suppressed in their simulations compared to our simulations with the **NSeg** clusters (Figure 3). This further supports the notion that the level of observed mass segregation in the Arches cluster cannot have a fully dynamical origin.

3.2. Choice of IMF and Implications for Collisional Runaway

In general we find that for the clusters with primordial mass-segregation (set **Seg**) the number of collisions is always significantly larger compared to the clusters with a standard Kroupa IMF without any primordial mass segregation (set **NSeg**; see Table 1), for example, in the case $W_0 = 8$ by more than a factor of two (30 for run SW8-1 and 14 for run NSW8-1) within the first 4 Myr. This is mainly due to the top-heaviness of the Arches IMF within $r \leq 2r_c$ (§2) and the larger overall mass of our clusters with primordial mass segregation, resulting in a larger number of massive stars with large collision cross sections. Consequently, the runaway growth of a massive star is much more likely to take place in clusters from set **Seg**.

As an example, Figure 4 shows the mass of the two most massive stars over time for the cluster with the **Seg** IMF (run SW8-1) and the **NSeg** IMF (run NSW8-1). In the **Seg** case there is a clear evidence of a collisional run-

away producing two very massive stars. The most massive star in this case attains a mass of $800 M_\odot$ through 12 successive collisions. The second most massive star also grows significantly and reaches $300 M_\odot$ through 4 successive collisions. A clear sign of a collisional runaway is a steep increase of the stellar mass through successive collisions. Figure 4 clearly shows that at $t_{cl} \simeq 2$ Myr the most massive star enters a runaway regime. The whole process of the runaway takes place between ~ 2 –4 Myr. In case of **NSeg** IMF the two most massive stars experience only two to three collisions and there is no runaway happening. We obtain qualitatively similar results when changing the random seed to generate other equivalent initial conditions. For instance, in the run SW8-2 with **Seg** IMF we see a runaway, where the most massive star grows to $\sim 10^3 M_\odot$ within the first 4 Myr starting from about $90 M_\odot$, through 17 successive collisions. The corresponding run with the **NSeg** IMF, NSW8-2, did not exhibit any runaway growth (Table 1). A similar result is obtained for simulated clusters with other W_0 values. For example, Figure 5 shows the growth of the two most massive stars in the simulated clusters for runs SW7-1 and NSW7-1, both clusters with $W_0 = 7$, but the first from the **Seg** and the latter from the **NSeg** set. Again, the run from set **Seg** shows clear evidence of a collisional runaway, whereas the equivalent cluster from set **NSeg** shows none. (For a full list of simulation results with other initial W_0 values, see Table 1.) Note that, in the collisional runaway of the stars in our simulations, we find that the stars can grow even after 3 Myr via collisions. This is due to the collisional rejuvenation prescription in BSE, which assumes complete mixing (Hurley et al. 2000). Thus the collisional stars live longer compared to their normal lifetime. This assumption is of course a simplification and the amount of mixing and thus rejuvenation depends on the details of the kinematics of the collisions (e.g., Sills et al. 1997; Glebbeek & Pols 2008). However, this assumption gives an upper limit of the degree of rejuvenation and lets the stars grow for a longer time than with a more realistic rejuvenation prescription. In this study for the considerations of a collisional runaway we take collisional sequences only upto $t_{cl} = 4$ Myr.

A very interesting aspect of these results with the **Seg** IMF is that, many of these runs lead to a double collisional runaway, one being stronger than the other (e.g., runs SW8-1,2, SW7-1,2; see Table 1 for a full list) creating two very massive stars (VMS). Double runaways have been studied and observed in some previous simulations with primordial binaries (e.g., Gürkan et al. 2006), however, a double runaway even without primordial binaries has not been observed before. Due to the flat mass spectrum in the high mass end of the **Seg** IMF, there is a larger reservoir of high-mass stars increasing the chance of a double runaway. A double runaway does not necessarily mean black hole binaries, as discussed in Gürkan et al. (2006), since the two VMSs may still collide with each other at a later time but before compact object formation (e.g., SW8-2, SW7-1). The signature of a double runaway and production of two VMSs seems to be common in all of our simulations with the **Seg** IMF, where the initial concentration is conducive to a collisional runaway, in particular for runs with King con-

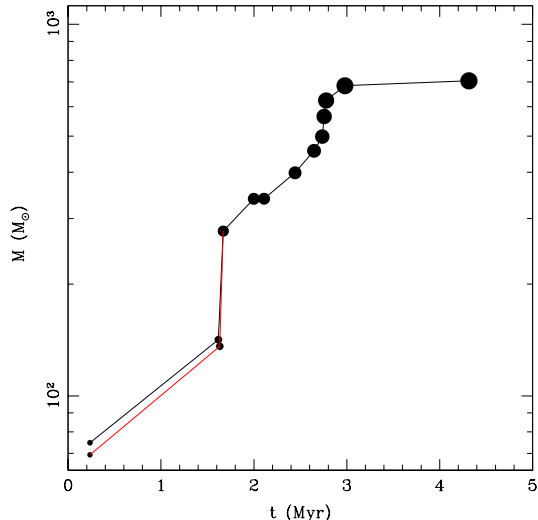


FIG. 5.— Same as Figure 4 but for runs SW7-1 and NSW7-1. No star in run NSW7-1 grows to $> 100 M_{\odot}$ within the first 4 Myr, hence are not shown on this plot.

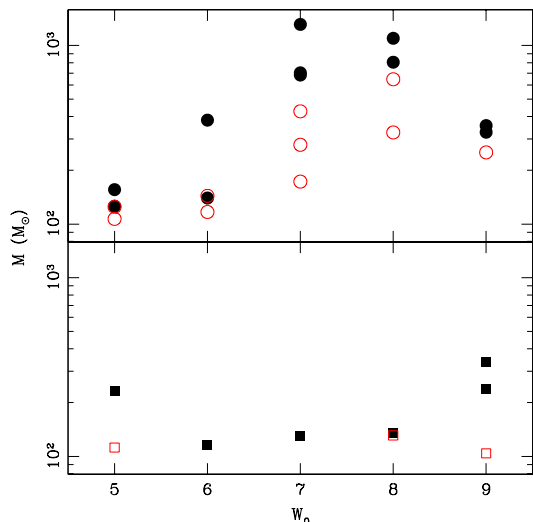


FIG. 6.— Masses of the two most massive stars are shown for each simulated cluster with the Seg (top panel) and NSeg (bottom panel) IMFs as a function of the initial King concentration parameter W_0 . The filled point and the open point show the highest and the second highest mass attained during the first 4 Myr of evolution. Cases where the mass is not above $100 M_{\odot}$ are not shown since the initial high mass cut-off of the IMF is $100 M_{\odot}$ in our simulations. Multiple realizations of the same cluster in each case is simulated to ascertain robustness against statistical fluctuations. Note that for the Seg IMF with $W_0 = 7$ and 8 , there is clear indication of double runaways.

centration parameters $W_0 = 7, 8, 9$ (Figure 6).

Similar results are obtained for clusters with other initial concentrations or W_0 values. The main difference is in the final mass of the most massive stars, shown in Figure 6. The final stellar mass is also subject to statistical fluctuations to a certain extent. The collisional runaway with the Seg IMF and $W_0 = 6$ is weak, whereas, for $W_0 = 5$ there is no runaway (Table 1). For each of

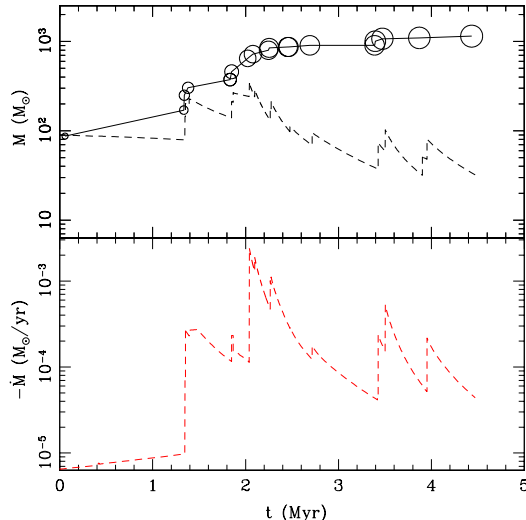


FIG. 7.— Effect of wind mass loss for the run SW8-2. Top panel: Solid line shows the mass growth via collision with the standard stellar evolution prescription in Nbody4. The circles show the time when the collisions happened. The dashed line shows the same collision chain, only with the high wind mass loss prescription (Glebbeek et al. 2009). Following each collision, the collision product is evolved and wind mass loss is taken into account. Bottom panel: The wind mass loss rate as a function of time.

these runs with the Seg IMF, the corresponding simulations with the same initial W_0 but the NSeg IMF do not exhibit any runaway and do not produce the VMSs. However, for $W_0 = 9$, both the Seg and the NSeg IMF simulations show runaways and the masses of the collisionally created most massive stars are comparable. In the Seg case $W_0 = 9$ shows a weaker collisional runaway in our simulated examples. This is because from a King model with $W_0 = 8$ to one with $W_0 = 9$, the core radius decreases considerably, thus the top-heavy IMF is within a smaller volume. As a result the total initial mass as well as the number of high-mass stars decrease. From our simulations, we find that with the Seg IMF, $W_0 = 7$ and 8 are optimal for strong collisional runaways. On one hand a lower W_0 decreases the probability of a runaway because of the lower central density. On the other hand, a higher W_0 gives the same result although the central density is higher, because of the lower overall mass of the cluster as well as the lower number of high-mass stars.

3.3. Enhanced Mass Loss via Stellar Winds

High-mass stars can lose a significant fraction of their mass through stellar winds (e.g., Cassinelli 1979; Chiosi & Maeder 1986; Kudritzki & Puls 2000). Glebbeek et al. (2009) show that a VMS generated via stellar collisions may lose mass through stellar winds at such a high rate that its collisional growth may be quenched. We explore this possibility, following their work, for our simulated clusters SW8-1 and SW8-2, where collisional runaways have been observed. Following Glebbeek et al. (2009) each collision is treated using the “Make Me a Massive Star” (MMAMS) software package (Gaburov et al. 2008; Lombardi et al. 2002), which gives the properties of the collision product. This output is then imported into the Eggleton stellar evolution code (Eggleton 1971, 1972; Pols et al. 1995) using the method

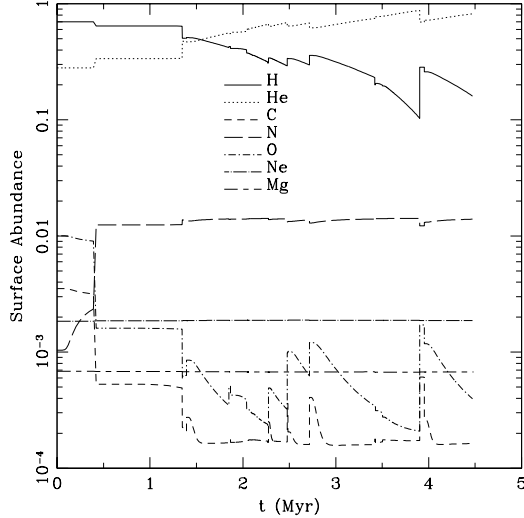


FIG. 8.— Time evolution of the surface abundance of the most massive star in the run SW8-2. Surface abundance of Hydrogen (H), Helium (He), Carbon (C), Nitrogen (N), Oxygen (O), Neon (Ne), and Magnesium (Mg) are shown. Note the very high surface abundance of Helium.

of Glebbeek et al. (2008). This method is repeated for every collision in the collision chain (for a more detailed description see Glebbeek et al. 2009, especially Section 2.1).

Figure 7 shows the time evolution of the most massive star for the run SW8-2 as an example. The solid line in the top panel shows the collisional growth of the stellar mass in the runaway observed in our run SW8-2, using the standard wind prescriptions from BSE/SSE, included in NBODY4. The dashed line in the top panel tracks the mass of the star assuming the wind mass loss prescriptions suggested by Glebbeek et al. (2009). The bottom panel shows the mass loss rate via stellar winds as a function of time according to Glebbeek et al. (2009). With this wind mass loss prescription, while collisions increase the stellar mass, the increased stellar mass in turn leads to enhanced wind mass loss. The growth of the stellar mass through the chain of collisions is quenched and instead of the $\sim 10^3 M_{\odot}$ VMS a star of only $\sim 30 M_{\odot}$ is produced with this wind prescription. At the final stage the star is burning Helium in its core and has a high surface Helium abundance ($X_{He,S} \gtrsim 0.8$) (Figure 8). We should mention that the modeling of stellar winds from high-mass stars is quite uncertain, and various treatments often come from extrapolations from observed stars at a lower mass. Depending on the prescription wind mass loss rates may vary by orders of magnitude. If indeed the high wind mass loss prescription is correct, then a VMS will not be produced even when a collisional runaway takes place. Interestingly, the mass lost via stellar winds due to the collisional growth of the stars will be extremely Helium rich which may provide observable signatures (more on this in §4.3). Similar results are obtained from the collision chain in run SW8-1.

4. POSSIBLE OBSERVATIONAL SIGNATURES OF A COLLISIONAL RUNAWAY

Here we discuss the possible observable signatures of a collisional runaway in a cluster. In the previous section

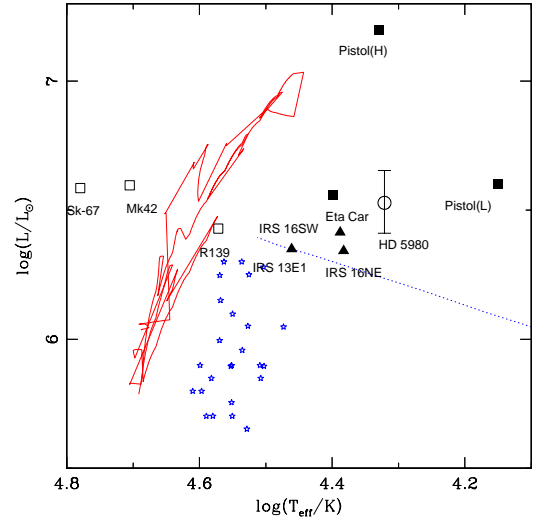


FIG. 9.— The evolution of the most massive star created in run SW8-2 in the luminosity (L) vs effective temperature (T_{eff}) plane. Solid red line shows the evolution of the most massive star for the enhanced wind mass loss prescription. The dotted line (blue) shows the Humphreys-Davidson limit (Humphreys & Davidson 1979). The filled black squares denote LBVs, open squares denote observed OB stars in the Magellanic clouds, filled triangles denote stars in GCs (Figer et al. 1998, and the references therein). Two points for the Pistol star denote high (H) and low (L) luminosity models (Figer et al. 1998). The blue pentagons show the observed bright stars in Arches (Clark et al. 2009, and the references therein).

we have shown that depending on the stellar wind prescription a collisional runaway may create a VMS or the mass growth can be quenched through high wind mass loss. Here we consider both cases and discuss possible observable signatures of both possibilities.

4.1. Possible Creation of another Pistol Star

The Quintuplet cluster is very similar to the Arches cluster. It is also very near the Galactic center (projected distance $\lesssim 40$ pc; e.g., Nagata et al. 1990; Portegies Zwart et al. 2002). The Arches and the Quintuplet are also similar in their metallicities, and mass (Najarro et al. 2009). The Arches is younger (2 ± 1 Myr) than the Quintuplet cluster (~ 4 Myr). The Pistol star is one of the most interesting and well studied objects in the Quintuplet. This is one of the brightest stars ever observed (Figure 9; Moneti et al. 1994; Cotera et al. 1996; Lang et al. 1997; Figer et al. 1998). The inferred initial mass of the Pistol star is $200 - 250 M_{\odot}$. The Pistol star is classified as a luminous blue variable (LBV Figer et al. 1998) or a B[e] (Morris et al. 1996) star. The stellar surface is extremely Helium rich and it has lost a significant fraction of its mass via Helium rich massive stellar winds (e.g. Figer et al. 1995; Cotera et al. 1996; Timmermann et al. 1996; Lang et al. 1997; Figer et al. 1998). From our results we find that the massive stars generated via collisional runaways may be a potential channel to produce a massive and Helium rich Pistol like star (Figure 7, 8). Figure 9 shows the evolution of the most massive star found in run SW8-2 for the enhanced wind mass loss case as an example. The massive star produced through the collisional runaway spends a significant period of time (e.g., $1.4 - 2.3$ Myr in case

of the run SW8-2) above the Humphreys-Davidson limit (Humphreys & Davidson 1979) like the Pistol star. Thus if the Arches was indeed created with a top-heavy IMF at the center as is observed today, then a Pistol-like star could be created at some point. However, due to the uncertainty in the age estimate of the Arches cluster and the onset of the collisional runaway in simulations depending on the initial conditions it is not possible to predict whether a similar LBV star should already have been created in the Arches cluster and could be observed today.

4.2. IMBH Progenitors

The presence of supermassive black holes at the center of most galaxies is now well established (e.g., Richstone et al. 1998; Kormendy & Gebhardt 2001; Ghez et al. 2005). Extrapolating the relation between the host mass and the black hole mass it has been postulated that massive clusters may also host black holes in the mass range $10^2 - 10^4 M_\odot$ (e.g., see reviews by van der Marel 2004; Rasio et al. 2004). These black holes are much less massive than the supermassive black holes at the centers of most galaxies but more massive than the stellar-mass black holes expected as remnants from high-mass stars. Although no conclusive observational evidence for an IMBH has been obtained yet, there are several interesting candidates (e.g., Farrell et al. 2009; Irwin et al. 2009). The main proposed channel of formation for these IMBHs is through collisional runaways in dense clusters (e.g., Freitag & Benz 2002; Portegies Zwart & McMillan 2002; Gürkan et al. 2004, 2006; Freitag et al. 2006b,a, 2007, 2006a,b). It is thus exciting to find young star clusters where a collisional runaway may have taken place.

The simulated clusters with the Seg IMF, in particular with $W_0 = 7, 8,$ and 9 create VMSs via collisional runaway. The counterparts of the same clusters with the more standard NSeg IMF do not produce these VMSs. If the winds do not quench the mass growth via collisions, then the VMSs can potentially be IMBH progenitors (e.g. Fryer 1999; Fryer & Kalogera 2001; Portegies Zwart & McMillan 2002; Heger et al. 2005; Belczynski et al. 2009). If an IMBH is indeed produced, there can be many observational signatures. Even without primordial binaries, at the high densities attained at the core binaries can form dynamically from three-body interactions. IMBHs being a lot more massive than the typical stars in its vicinity inevitably exchange into a binary or a higher order bound system (Gill et al. 2008). A stable mass transfer to the IMBH from its binary companion can be visible as ultra luminous X-ray sources. Inspiral and capture of compact objects such as stellar mass black holes and neutron stars into the IMBH can be a strong gravity wave source detectable with the Laser Interferometric Space Antennae (LISA). The simulated clusters with the Seg IMF, often show signatures of two separate runaways, one weaker than the other. These runaways may produce two VMSs, both of which may create massive black holes. If the VMSs do not collide prior to creating the massive black holes a massive binary black hole system can be formed. If produced, an IMBH-IMBH binary is a good source for LISA during the inspiral phase (see Gürkan et al. 2006).

4.3. Enhanced Wind Mass Loss: Helium Enrichment

If the wind mass loss of the most massive star dominates over its collisional growth, then the rapid increase in mass is inhibited. (Figure 7). In this case a VMS is not produced as a result of the runaway. Instead, a large amount of processed stellar material is injected into the surrounding interstellar medium, which is, consequently, expected to become strongly enriched in Helium. For example, the total mass lost via winds from the most massive star formed in the runaway in the run SW8-2 is $\sim 10^3 M_\odot$, while its $X_{He,S}$ can exceed 0.9, resulting in $\approx 500 M_\odot$ of Helium ejected via winds. In contrast, if the stars, that merged to form the VMS, are evolved in isolation, the total mass of ejected Helium would be significantly lower, $\approx 100 M_\odot$, within the first 3 Myr. An anomalously high Helium enrichment of the surrounding interstellar medium may, therefore, provide an observational signature for a collisional runaway.

However, such a signature might not necessarily be found inside Arches but rather outside of it, as the material lost through winds has rather large velocities. Assuming the terminal flow velocity of the wind from O/B stars for solar metallicities is 0.5 times the escape speed from the surface of the star (Vink et al. 2001), we find that the wind velocity for our collisionally formed VMSs is ≈ 500 km/s. As these velocities are much larger than the escape speed of even much more massive star clusters, it is likely that the material escapes the Arches cluster entirely. On the other hand, this material can also slow down through collisions with winds from other massive stars. Such multiple stellar wind interactions result in a complex network of shock compressed, extremely hot ($10^7 - 10^8 K$) gas that should then leave the cluster as a cluster wind (see, e.g., Canto et al. 2000). The structure of this wind consists of four zones (Silich et al. 2004): a star cluster region filled with a hot X-ray plasma, an X-ray halo with decreasing temperature profile, a line-cooling, recombining zone, and a region of recombined gas, exposed to the UV radiation from the central star cluster. Indeed diffuse X-ray bright sources have been observed within Arches as well as extending beyond the cluster radius (e.g. Yusef-Zadeh et al. 2002; Rockefeller et al. 2005). This extremely hot gas may also be confined due to ram pressure exerted by a molecular cloud or other external medium surrounding the cluster (Rockefeller et al. 2005).

Helium abundances are usually determined through measuring Helium recombination lines (e.g., Peimbert et al. 2000). Thus a strong Helium enrichment can then only be detected outside the X-ray halo region, in the line cooling zone. Based on detailed calculations of Silich et al. (2004), this region is outside a radius of 3-7 pc from the Arches cluster. Other signatures of a collisional runaway might be provided by the wind structure itself. This is because the extension and physical parameters of the diffuse X-ray emitting region are mainly dependent on the sum of the mass-loss rates of the individual sources. Given that for the case of a runaway this mass loss rate can be significantly increased, it may strongly influence the appearance of the cluster winds. However, such imprints might be very difficult to detect. This is in part because our rates for the most massive star are highly time-variable,

varying by two orders of magnitudes within a few 10^5 yr, while particularly large values in excess of the total mass injection rate for all other Arches stars of $7 \approx \times 10^{-4} M_{\odot} \text{ yr}^{-1}$ (Stevens & Hartwell 2003) are only attained during an even shorter timescale. Another reason is that the Arches cluster wind may be confined by cooler surrounding inter stellar material, an effect that is hard to quantify (Rockefeller et al. 2005).

Instead of searching for imprints of a runaway in the global cluster wind structure, signatures may be found in the properties of individual objects, as stellar radii and mass loss rates of runaway stars can be unusual (Figure 7; Glebbeek et al. 2009). One way to directly detect and constrain the mass loss rate, the effective radius of the star, and the wind velocities is by exploiting the so called Baldwin effect (Baldwin 1977; Morris et al. 1993), which is an anticorrelation between the line luminosity of one strong emission line, such as HeII (often found in WR winds), and the continuum luminosity. van Gent et al. (2001) show that the ratio of line and continuum luminosity, the equivalent width W , depends on the mass loss rate, \dot{M} , the terminal velocity of the wind, v_{∞} , and the effective radius, R_{\star} , as $W \propto \dot{M}^2 v_{\infty}^{-2} R_{\star}^{-3}$. When the distance of the star is known, and the temperature can be estimated, observation of W can constrain the wind mass loss rate, wind velocities and the effective radii of the stars.

5. SUMMARY AND CONCLUSION

We carried out many N -body simulations with initial conditions chosen such as to resemble the Arches cluster. Using a standard Kroupa (2001) IMF with no radial variation (NSeg) and a radially dependent IMF that corresponds to the level of mass segregation inferred from observations (Seg; e.g. Dib et al. 2007a), we study possible consequences and discuss potential observable signatures to distinguish between the two cases.

We show that the degree of mass segregation via dynamical evolution of the simulated clusters during the first 2 Myr is minor both for the Seg and the NSeg IMF (Figure 2). Thus, while runs with the Seg IMF reproduce well all parts of the currently observed slopes in the MF at ≈ 2 Myr, those with the NSeg IMF do not produce enough mass segregation within the Arches lifetime to match the observed MF as well (Figure 2). Therefore, our results indicate that the present day observed degree of mass segregation in the Arches cluster cannot be a result of dynamics only and at least some degree of primordial mass segregation is required.

We further show that the choice of IMF changes the overall dynamical evolution significantly for Arches like clusters over a range of initial W_0 . For the Seg IMF there is clear evidence of collisional runaway, producing stars up to $\sim 10^3 M_{\odot}$ over a range of initial concentrations (Table 1, Figures 4, 5, 6). In contrast, with the more standard NSeg IMF no collisional runaway is observed with the same initial conditions. We find that the sequence of collisions in the simulations with successful collisional runaway starts at around 2 Myr. Note that the current estimated age of the Arches is 2 ± 1 Myr (e.g., Stolte et al. 2002). Hence, if the observed top-heavy MF within $r \sim 2r_c$ is indeed primordial, then it is possible that a collisional runaway has started or is bound to happen. Unfortunately, the uncertainty in the

age estimation prevents us from predicting whether a collisional runaway should already have taken place in the Arches.

An interesting aspect of the collisional runaways observed in this study is the general tendency of a double runaway in cases where the collisional runaway is strong (e.g., runs SW8-1,2 and runs SW7-1,2, see Table 1). Double collisional runaways have been observed and studied in numerical simulations before (Gürkan et al. 2006). However, those simulations concluded that primordial binaries are a necessity for a double collisional runaway. It is very interesting that with the primordially mass-segregated clusters even without any primordial binaries double collisional runaways can take place. Due to the flatness in the high mass end of the IMF in this case, there is a larger reservoir of high-mass stars. Thus the probability to start a second runaway is higher. The ultimate fate of the smaller runaway is dependent on the statistical fluctuations of the simulation (see §3). However, it is possible that the VMSs do not collide prior to compact object formation and both stay bound to the cluster after their respective supernova explosions (e.g., run SW8-1). In such a case they may form IMBH binaries or coalesce at the center of the cluster. If possible to form, this can create a very strong gravity wave signal for LISA (Gürkan et al. 2006).

If the mass loss from stellar evolution driven winds is too high then the collisional mass growth is quenched (Glebbeek et al. 2009). By evolving the collision products separately following each successive collision in a sequence of runaway collisions according to the prescription in Glebbeek et al. (2009) we find that the VMSs are not produced as a result of a collisional runaway. Instead, a Helium star of a few tens of a Solar mass is created (Figure 7). The mass lost via these winds is extremely Helium rich, with $X_{He,S}$ reaching beyond 0.9. In this case the cluster as well as its surrounding medium will be enriched by this Helium rich gas, which could be observed through recombination at distances beyond 3 – 7 pc from the Arches cluster.

Further indications of a collisional runaway might be provided by the runaway object itself, as such an object has a rather unusual radius and mass loss rate compared to ordinary massive stars. Constraints on the radius, mass loss rate, and the wind speeds may be obtained using the Baldwin effect (e.g., Baldwin 1977; van Gent et al. 2001). Furthermore, during the evolution of the runaway star, a Pistol like stellar object may also be produced (§4.1). However, since the duration for which the star attains Pistol like high luminosities is short, it is not possible to predict whether a Pistol like star should already have been created in Arches given the uncertainties in the age estimation and the statistical fluctuations in the exact onset and the details of the simulated collisional runaways.

Nevertheless, we should point out that the above recipe to follow the runaway star for these high stellar winds is not completely self-consistent. Each collision in a cluster is dependent on the masses and radii of the collision progenitors. Since, severe wind mass loss from the stars changes the masses of the stars significantly, the chain of collisions in the runaway may also be different. However, this model still provides us with an estimate of the total mass loss from the VMS via stellar winds, its stel-

lar properties, as well as the composition of the ejected material if a runaway did indeed happen.

We thank Farhad Yusef-Zadeh for helpful suggestions. This research was supported by NASA Grant NNX08AG66G and NSF Grant AST-0607498 at North-

western University. This research was partly done at KITP while the authors participated in the spring 2009 program on “Formation and Evolution of Globular Clusters”, and was supported in part by the NSF Grant PHY05-51164.

REFERENCES

- Aarseth, S. J. 2003, *Gravitational N-Body Simulations*, ed. S. J. Aarseth
- Baldwin, J. A. 1977, *ApJ*, 214, 679
- Baumgardt, H., De Marchi, G., & Kroupa, P. 2008, *ApJ*, 685, 247
- Belczynski, K., Bulik, T., Fryer, C. L., Ruiter, A., Vink, J. S., & Hurley, J. R. 2009, arXiv:0904.2784v1 [astro-ph.SR]
- Bonnell, I. A. & Davies, M. B. 1998, *MNRAS*, 295, 691
- Canto, J., Raga, A. C., & Rodriguez, L. F. 2000, *The Astrophysical Journal*, 536, 896
- Cassinelli, J. P. 1979, *ARA&A*, 17, 275
- Chiosi, C. & Maeder, A. 1986, *ARA&A*, 24, 329
- Clark, J. S., Crowther, P. A., & Mikles, V. J. 2009, arXiv:0909.3818v1 [astro-ph.SR]
- Cotera, A. S., Erickson, E. F., Colgan, S. W. J., Simpson, J. P., Allen, D. A., & Burton, M. G. 1996, *ApJ*, 461, 750
- Dabringhausen, J., Kroupa, P., & Baumgardt, H. 2009, *MNRAS*, 394, 1529
- Demleitner, M., Accomazzi, A., Eichhorn, G., Grant, C. S., Kurtz, M. J., & Murray, S. S. 2001, in *Astronomical Society of the Pacific Conference Series*, Vol. 238, *Astronomical Data Analysis Software and Systems X*, ed. F. R. Harnden, Jr., F. A. Primini, & H. E. Payne, 321
- Dib, S. 2007, *Journal of Korean Astronomical Society*, 40, 157
- Dib, S., Kim, J., & Shadmehri, M. 2007a, *MNRAS*, 381, L40
- Dib, S., Kim, J., Vázquez-Semadeni, E., Burkert, A., & Shadmehri, M. 2007b, *ApJ*, 661, 262
- Eggleton, P. P. 1971, *MNRAS*, 151, 351
- . 1972, *MNRAS*, 156, 361
- Elmegreen, B. G. 2004, *MNRAS*, 354, 367
- Elmegreen, B. G. & Shadmehri, M. 2003, *MNRAS*, 338, 817
- Farrell, S. A., Webb, N. A., Barret, D., Godet, O., & Rodrigues, J. M. 2009, *Nature*, 460, 73
- Figer, D. F., Kim, S. S., Morris, M., Serabyn, E., Rich, R. M., & McLean, I. S. 1999, *ApJ*, 525, 750
- Figer, D. F., McLean, I. S., & Morris, M. 1995, *ApJ*, 447, L29
- Figer, D. F., Najarro, F., Morris, M., McLean, I. S., Geballe, T. R., Ghez, A. M., & Langer, N. 1998, *ApJ*, 506, 384
- Freitag, M. & Benz, W. 2002, *A&A*, 394, 345
- Freitag, M., Guerkan, M. A., & Rasio, F. A. 2007, in *Astronomical Society of the Pacific Conference Series*, Vol. 367, *Massive Stars in Interactive Binaries*, ed. N. St.-Louis & A. F. J. Moffat, 707
- Freitag, M., Gürkan, M. A., & Rasio, F. A. 2006a, *MNRAS*, 368, 141
- Freitag, M., Rasio, F. A., & Baumgardt, H. 2006b, *MNRAS*, 368, 121
- Fryer, C. L. 1999, *ApJ*, 522, 413
- Fryer, C. L. & Kalogera, V. 2001, *ApJ*, 554, 548
- Gaburov, E., Lombardi, J. C., & Portegies Zwart, S. 2008, *MNRAS*, 383, L5
- Ghez, A. M., Salim, S., Hornstein, S. D., Tanner, A., Lu, J. R., Morris, M., Becklin, E. E., & Duchêne, G. 2005, *ApJ*, 620, 744
- Gieles, M. & Baumgardt, H. 2008, *MNRAS*, 389, L28
- Gill, M., Trenti, M., Miller, M. C., van der Marel, R., Hamilton, D., & Stiavelli, M. 2008, *ApJ*, 686, 303
- Glebbeek, E., Gaburov, E., de Mink, S. E., Pols, O. R., & Portegies Zwart, S. F. 2009, *A&A*, 497, 255
- Glebbeek, E. & Pols, O. R. 2008, *A&A*, 488, 1017
- Glebbeek, E., Pols, O. R., & Hurley, J. R. 2008, *A&A*, 488, 1007
- Gürkan, M. A., Fregeau, J. M., & Rasio, F. A. 2006, *ApJ*, 640, L39
- Gürkan, M. A., Freitag, M., & Rasio, F. A. 2004, *ApJ*, 604, 632
- Gürkan, M. A. & Rasio, F. A. 2005, *ApJ*, 628, 236
- Heger, A., Woosley, S. E., & Baraffe, I. 2005, in *Astronomical Society of the Pacific Conference Series*, Vol. 332, *The Fate of the Most Massive Stars*, ed. R. Humphreys & K. Stanek, 339
- Hillenbrand, L. A. & Hartmann, L. W. 1998, *ApJ*, 492, 540
- Humphreys, R. M. & Davidson, K. 1979, *ApJ*, 232, 409
- Hurley, J. R., Pols, O. R., & Tout, C. A. 2000, *MNRAS*, 315, 543
- Hurley, J. R., Tout, C. A., & Pols, O. R. 2002, *MNRAS*, 329, 897
- Irwin, J. A., Brink, T., Bregman, J. N., & Roberts, T. P. 2009, arXiv:0908.1115v1
- Kim, S. S., Figer, D. F., Kudritzki, R. P., & Najarro, F. 2006, *ApJ*, 653, L113
- . 2007, *Journal of Korean Astronomical Society*, 40, 153
- Kim, S. S. & Morris, M. 2003, *ApJ*, 597, 312
- King, I. R. 1966, *AJ*, 71, 64
- Kormendy, J. & Gebhardt, K. 2001, in *American Institute of Physics Conference Series*, Vol. 586, *20th Texas Symposium on relativistic astrophysics*, ed. J. C. Wheeler & H. Martel, 363–381
- Kroupa, P. 2001, *MNRAS*, 322, 231
- Krumholz, M. R., McKee, C. F., & Tumlinson, J. 2009, *ApJ*, 699, 850
- Kudritzki, R.-P. & Puls, J. 2000, *ARA&A*, 38, 613
- Lang, C. C., Goss, W. M., & Wood, D. O. S. 1997, *ApJ*, 474, 275
- Lombardi, Jr., J. C., Warren, J. S., Rasio, F. A., Sills, A., & Warren, A. R. 2002, *ApJ*, 568, 939
- Miller, G. E. & Scalo, J. M. 1979, *ApJS*, 41, 513
- Moneti, A., Glass, I. S., & Moorwood, A. F. M. 1994, *MNRAS*, 268, 194
- Morris, P., Conti, P. S., Lamers, H. J. G. L. M., & Koenigsberger, G. 1993, *ApJ*, 414, L25
- Morris, P. W., Eenens, P. R. J., Hanson, M. M., Conti, P. S., & Blum, R. D. 1996, *ApJ*, 470, 597
- Nagata, T., Woodward, C. E., Shure, M., & Kobayashi, N. 1995, *AJ*, 109, 1676
- Nagata, T., Woodward, C. E., Shure, M., Pipher, J. L., & Okuda, H. 1990, *ApJ*, 351, 83
- Najarro, F., Figer, D. F., Hillier, D. J., Geballe, T. R., & Kudritzki, R. P. 2009, *ApJ*, 691, 1816
- Nakano, T. 1966, *Progress of Theoretical Physics*, 36, 515
- Peimbert, M., Peimbert, A., & Ruiz, M. T. 2000, *ApJ*, 541, 688
- Pols, O. R., Tout, C. A., Eggleton, P. P., & Han, Z. 1995, *MNRAS*, 274, 964
- Portegies Zwart, S., Gaburov, E., Chen, H.-C., & Gürkan, M. A. 2007, *MNRAS*, 378, L29
- Portegies Zwart, S. F., Makino, J., McMillan, S. L. W., & Hut, P. 2002, *ApJ*, 565, 265
- Portegies Zwart, S. F. & McMillan, S. L. W. 2002, *ApJ*, 576, 899
- Rasio, F. A., Freitag, M., & Gürkan, M. A. 2004, in *Coevolution of Black Holes and Galaxies*, ed. L. C. Ho, 138
- Richstone, D., Ajhar, E. A., Bender, R., Bower, G., Dressler, A., Faber, S. M., Filippenko, A. V., Gebhardt, K., Green, R., Ho, L. C., Kormendy, J., Lauer, T. R., Magorrian, J., & Tremaine, S. 1998, *Nature*, 395, A14
- Rockefeller, G., Fryer, C. L., Melia, F., & Wang, Q. D. 2005, *ApJ*, 623, 171
- Salpeter, E. E. 1959, *ApJ*, 129, 608
- Serabyn, E., Shupe, D., & Figer, D. F. 1998, *Nature*, 394, 448
- Silich, S., Tenorio-Tagle, G., & Rodríguez-González, A. 2004, *ApJ*, 610, 226
- Silk, J. & Takahashi, T. 1979, *ApJ*, 229, 242
- Sills, A., Lombardi, Jr., J. C., Bailyn, C. D., Demarque, P., Rasio, F. A., & Shapiro, S. L. 1997, *ApJ*, 487, 290
- Stevens, I. R. & Hartwell, J. M. 2003, *MNRAS*, 339, 280
- Stolte, A. 2006, *Journal of Physics Conference Series*, 54, 217
- Stolte, A., Ghez, A. M., Morris, M., Lu, J. R., Brandner, W., & Matthews, K. 2008, *ApJ*, 675, 1278
- Stolte, A., Grebel, E. K., Brandner, W., & Figer, D. F. 2002, *A&A*, 394, 459
- Subramaniam, A., Sagar, R., & Bhatt, H. C. 1993, *A&A*, 273, 100
- Tan, J. C., Krumholz, M. R., & McKee, C. F. 2006, *ApJ*, 641, L121
- Timmermann, R., Genzel, R., Poglitsch, A., Lutz, D., Madden, S. C., Nikola, T., Geis, N., & Townes, C. H. 1996, *ApJ*, 466, 242

van der Marel, R. P. 2004, in *Coevolution of Black Holes and Galaxies*, ed. L. C. Ho, 37
van Gent, J. I., Lamers, H. J. G. L. M., de Koter, A., & Morris, P. W. 2001, *A&A*, 372, 963
Vink, J. S., de Koter, A., & Lamers, H. J. G. L. M. 2001, *A&A*, 369, 574

Yusef-Zadeh, F., Law, C., Wardle, M., Wang, Q. D., Fruscione, A., Lang, C. C., & Cotera, A. 2002, *ApJ*, 570, 665